Inverse cascades in rotating stratified turbulence: Fast growth of large scales

2013 EPL 102 44006

(http://iopscience.iop.org/0295-5075/102/4/44006)

A Letters Journal Exploring the Frontiers of Physics

May 2013

EPL, **102** (2013) 44006
doi: 10.1209/0295-5075/102/44006

www.epljournal.org

Inverse cascades in rotating stratified turbulence: Fast growth of large scales

R. Marino[1], P. D. Mininni[1,2], D. Rosenberg[3] and A. Pouquet[1,4]

[1] *National Center for Atmospheric Research - P.O. Box 3000, Boulder, CO 80307, USA*
[2] *Departamento de Física, Facultad de Ciencias Exactas y Naturales, Universidad de Buenos Aires and IFIBA, CONICET - Ciudad Universitaria, 1428 Buenos Aires, Argentina*
[3] *National Center for Computational Sciences, Oak Ridge National Laboratory P.O. Box 2008, Oak Ridge, TN 37831, USA*
[4] *Department of Applied Mathematics, University of Colorado at Boulder - Boulder, CO 80309, USA*

received 11 March 2013; accepted in final form 17 May 2013
published online 11 June 2013

PACS 47.55.Hd – Stratified flows
PACS 47.32.Ef – Rotating and swirling flows
PACS 47.27.-i – Turbulent flows

Abstract – We examine the inverse cascade of kinetic energy to large scales in rotating stratified turbulence as occurs in the oceans and in the atmosphere, while varying the relative frequency of gravity to inertial waves, N/f. Using direct numerical simulations with grid resolutions up to 1024^3 points, we find that the transfer of energy from three-dimensional to two-dimensional modes is most efficient in the range $1/2 \leqslant N/f \leqslant 2$, in which resonances disappear. In this range, the cascade is faster than in the purely rotating case, and thus the interplay between rotation and stratification helps creating large-scale structures. The ensuing inverse cascade follows a $-5/3$ spectral law with an approximately constant flux. This inverse cascade becomes negligible when stratification is dominant.

Introduction. – Geophysical flows are turbulent, with complex systems of eddies interacting non-linearly, making such flows largely unpredictable. They also support strong waves, due to the combined effect of rotation and stratification [1]. A recent re-analysis of oceanic data and theoretical developments of weak turbulence points to a variety of dynamical regimes, depending on whether waves or eddies dominate, and emphasizing the importance non-linearities play once the geostrophic balance at large scale is broken [2]. The interactions between winds and waves have an important role in the planetary and oceanic boundary layers with dynamical consequences for transport and mixing of momentum, CO_2 and heat [3], and imperfect modeling of these interactions results in a Southern Ocean mixed layer which is too shallow in many climate models [4], thereby affecting the overall climate evolution [5]. Thus, a more detailed understanding of interactions between eddies and waves in these flows is in order.

Non-linear interactions occur both at small scales, with turbulent mixing, dissipation, and the occurrence of localized extreme events, as well as at large scales where accumulation of energy can take place through an inverse cascade. Inverse cascades are a well-known feature of non-linear dynamics, reviewed extensively in the context of two-dimensional (2D) Navier-Stokes fluids [6–9]. The reason for its occurrence can be explained with statistical mechanics in the ideal (non-dissipative) case: When there is more than one quadratic invariant, the equilibria that develop are not simply an equipartition among all modes of the truncated system, leading solely to accumulation of energy at small scales. Instead, other solutions can develop that see a pile-up of one of the invariants at large scale, be it energy in 2D fluids, or magnetic helicity in three-dimensional (3D) magnetodhydrodynamic, and this behavior is preserved in the dissipative case, including in the presence of forcing. It is also observed in 3D for flows in domains with non-unit aspect ratio, when they can be considered quasi-2D [10]. Direct and inverse turbulent cascades are also observed in outer space plasmas [11–13].

Similarly, in rotating turbulence, there is a crossover between a 3D behavior for weak rotation, to a quasi-2D behavior as the rotation rate gets above a threshold [14].

When including both rotation and stratification, as occurs in the Earth's atmosphere and oceans, several

phenomena can compete. In the presence of large-scale forcing (see, *e.g.*, [15–21]), inverse cascades cannot be observed due to insufficient scale separation. With small-scale excitation, conclusions are somewhat contradictory, in particular for weak rotation. When rotation and stratification are of comparable strength, $N \approx f$, with N the Brunt-Väisälä frequency and $f = 2\Omega$, Ω being the imposed solid-body rotation, inverse cascades do take place [22,23], and they are associated with geostrophic modes. In fact, in the limit of quasi-geostrophy considered by Charney [24], the conservation of potential vorticity also leads to an inverse cascade of energy which has been verified numerically (see [25]); note that $N/f \approx 5$ is found in the Southern Ocean at mid latitude [2]. In purely rotating turbulence, energy can cascade both to the large and to the small scales [14,26]. For negligible or no rotation, on the one hand an increase of vertical length scales was observed in simulations for times of the order of 10^3 turnover times [27,28], although long-time integrations suffer from many limitations, specially in periodic boxes in the presence of waves that can go across the domain multiple times. On the other hand, Waite and Bartello [29,30] conclude to the lack of an inverse cascade in the purely stratified case, mostly on the basis of an argument involving again statistical mechanics. At fixed stratification and for $N/f \geqslant 1$, all these authors find that the stronger the inverse cascade, the stronger the rotation, or, in other words, that for fixed rotation increasing the stratification only slows down the inverse cascade. The characteristic vertical scale increases with increasing rotation, reflecting the anisotropy of the dispersion relation of inertial-gravity waves (see below). In the framework of these studies, it is also concluded that there is little dependence on N/f, provided the waves are sufficiently strong, whereas using Rapid Distortion Theory (RDT) it was shown in [31] that, for example, the distribution among the horizontal, vertical and potential energy modes is governed by that ratio.

In this context, it is the purpose of this letter to demonstrate that i) the inverse cascade growth rate is non-monotonic in N/f, with behavior for $N/f < 1$ different for the one found for $N/f \geqslant 1$ in previous studies; ii) a moderate stratification (in the sense that $N/f \leqslant 2$) produces a faster growth of energy at large scale than in the purely rotating case, a growth characteristic of inverse cascades in quasi-2D flows; that iii) the efficiency of the accumulation of energy at large scale decreases rapidly with $N/f > 2$, and that when stable stratification is the dominant factor, as in many cases of atmospheric and oceanic dynamics, there is no such inverse cascade except possibly for transients.

Numerical set-up. – We integrate the incompressible Boussinesq equations, with solid-body rotation Ω and gravity g, anti-aligned in the vertical (z) direction, with θ the buoyancy (in units of velocity), P the pressure, ν the viscosity, and κ the diffusivity (the Prandtl number, ν/κ, is taken equal to unity):

$$\partial_t \mathbf{u} + \mathbf{u}\cdot\nabla\mathbf{u} - \nu\Delta\mathbf{u} = -\nabla P - N\theta e_z - 2\mathbf{\Omega}\times\mathbf{u} + \mathbf{F}_u, \quad (1)$$

$$\partial_t \theta + \mathbf{u}\cdot\nabla\theta - \kappa\Delta\theta = Nw, \quad (2)$$

$$\nabla\cdot\mathbf{u} = 0. \quad (3)$$

The velocity is $\mathbf{u} = (u, v, w)$, $\mathbf{\Omega} = \Omega e_z$, and $\mathbf{F}_u$ is a random and isotropic mechanical forcing with an amplitude chosen so that the r.m.s. velocity is $U_0 \approx 1$ in the absence of rotation and stratification, and applied in a spherical shell of modes with wave numbers k_F in Fourier space. Here, $N = [-g\partial_z\bar{\theta}/\theta]^{1/2}$ is the Brunt-Väisälä frequency, where $\partial_z\bar{\theta}$ is the background imposed stratification. In the absence of stratification, the inertial wave frequency is $\omega_{\mathbf{k}} = fk_\parallel/k$ with $f = 2\Omega$ and $k = |\mathbf{k}|$. In the purely stratified case, gravity waves satisfy $\omega_{\mathbf{k}} = Nk_\perp/k$ with $k_\perp = (k_x^2 + k_y^2)^{1/2}$, and in the general case

$$\omega_{\mathbf{k}} = k^{-1}\sqrt{N^2k_\perp^2 + f^2k_\parallel^2} \quad (4)$$

is the frequency of inertial-gravity waves (see, *e.g.*, [32]). The ideal incompressible Boussinesq equations with $\nu = \kappa = 0$ and $\mathbf{F}_u = 0$ conserve the potential vorticity $PV = -fN + f\partial_z b - N\omega_z + \omega\cdot\nabla b$ point-wise, as well as the total (kinetic + potential) energy $E_T = E_V + E_P$ in the entire volume. Although many studies of stratified turbulence consider 2D forcing, the choice of isotropic forcing is made in this letter since we vary N and f in a wide range, including the cases $N = 0$ and $f = 0$. As anisotropies that develop in purely rotating and purely stratified flows are of a different nature, the choice of isotropic forcing allows us not to favor any of the two regimes, and let anisotropy develop only through the dynamical evolution of the flow.

The equations are solved using the GHOST code which is pseudo-spectral with periodic boundary conditions in all directions and unit aspect ratio domains with length 2π. It is parallelized with a hybrid MPI/OpenMP method [33]. The Froude, Rossby and Reynolds numbers are defined, respectively, as $\mathrm{Fr} = U_0/[NL_F]$, $\mathrm{Ro} = U_0/[fL_F]$, and $\mathrm{Re} = U_0L_F/\nu$, with $L_F = 2\pi/k_F$ the forcing scale. The buoyancy Reynolds number is $\mathcal{R}_\mathcal{B} = \mathrm{ReFr}^2$; note that it can also be evaluated as $\epsilon/[\nu N^2]$, with $\epsilon = \langle\mathbf{u}\cdot\mathbf{F}_u\rangle$ the energy injection rate. In the simulations this number varies in the range $0.4 \leqslant \mathcal{R}_\mathcal{B} \leqslant 110$. Note that when $\mathcal{R}_\mathcal{B} = 1$, the Ozmidov scale L_{oz} is equal to the dissipation scale. L_{oz} is the scale at which the effect of stratification is small enough that an isotropic Kolmogorov range is recovered at smaller scales. In the simulations, its corresponding wave number $k_{oz} = 2\pi/L_{oz}$ varies between 200 and 5000. The Zeman wave number (the equivalent wave number for the effect of rotation) varies in a similar range.

Initial conditions in the simulations are $\theta = 0$ and an isotropic random velocity field centered around k_F. As the system is integrated, the energy first decays, and depending on whether an inverse cascade develops or not,

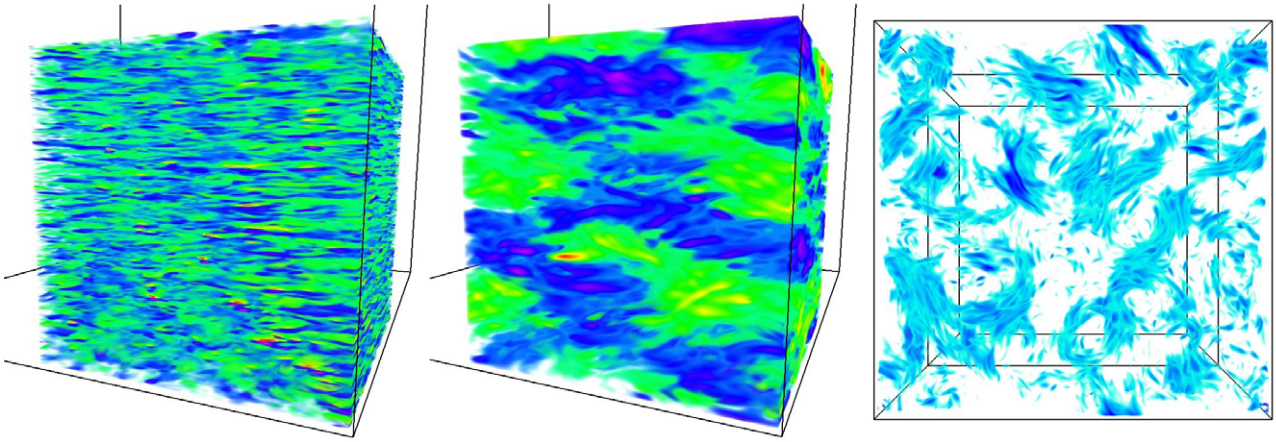

Fig. 1: (Colour on-line) Three-dimensional visualizations of the buoyancy θ in 1/8 of the entire volume for two 1024^3 runs at late times. $\mathrm{Fr} = 0.04$, with no rotation ($f = 0$, left) and with $N/f = 2$ (middle); in the former case, one sees layers which are thinner than the forcing length, whereas large-scale growth is detectable on the right, corresponding to an inverse cascade of energy. Dark colour (blue and red) corresponds to positive values of θ, and light colour (green and yellow) to negative values of θ. On the right is a top view in the entire box of regions with large horizontal kinetic-energy density $(u^2 + v^2)/2$, for $N/f = 2$ and $\mathrm{Fr} = 0.04$, showing the existence of large-scale structures which do not have the full depth of the box. The depth of these eddies is $\approx 1/8$ of the total box depth.

can either increase in time, or stabilize around a turbulent-steady-state value. In all the runs, the flow is left to evolve for at least 35 turnover times computed at the forcing scale, $\tau_{\mathrm{NL}} = L_F/U_F$ (with $U_F = \sqrt{k_F E_V(k_F)}$ the r.m.s. velocity at the forcing scale), and up to 130 turnover times in some cases.

Altogether, seventeen runs were performed, all of them but three on grids of $n_p^3 = 512^3$ points, with $k_F \in [22, 23]$ and $\nu = 2.73 \times 10^{-4}$, whereas $k_F \in [40, 41]$ for the three $n_p^3 = 1024^3$ runs and $\nu = 1.4 \times 10^{-4}$. These choices for the forcing wave number allow for sufficient scale separation to study the inverse-cascade scaling. All runs have $\mathrm{Re} \approx 1000$, and $N/f = 0$ (with $N = 0$), 1/4, 1/2, 3/2, 2, 3, 4, 7, or ∞ (with $f = 0$). These runs can be further divided into two sets: runs with constant Rossby number ($\mathrm{Ro} \approx 0.08$), and runs with constant Froude number ($\mathrm{Fr} \approx 0.04$).

Results. – In fig. 1 we show a perspective volume rendering of the buoyancy θ in 1/8 of the whole volume for two runs on grids of 1024^3 points, at late times. On the left is the flow without rotation ($f = 0$), and the main structure here is the layering of the buoyancy at a scale smaller than that of the forcing (possibly at the buoyancy scale). In the presence of rotation (middle, $N/f = 2$), larger-scale fluctuations are clearly observed that grow in time. On the right is given a top view of the horizontal energy density at the same time for the rotating stratified run. The entire box is shown, with the horizontal energy density only rendered for a depth of $\approx 1/8$ of the box (regions with low-energy density are transparent, so the structures can be seen at different depths). Large-scale columnar eddies with little variation in the vertical are visible, but the depth of these structures is $\approx 1/8$ of the box (*i.e.*, the vertical correlation length is smaller than 2π).

The difference between these two runs is further confirmed by the examination of the temporal evolution of kinetic energy, as well as of the total energy and integral scales in the flow. As an example, fig. 2 (top) shows the time evolution of E_V for several runs with $N/f = 0$, 1/2, 2, and 4, all with $\mathrm{Ro} \approx 0.08$, plus one in the purely stratified case ($f = 0$ and $\mathrm{Fr} \approx 0.04$). The unit of time is the eddy turn-over time τ_{NL} at the forcing scale in each specific run. Note that the early-time variations ($t/\tau_{\mathrm{NL}} < 1$) are dominated by stratification, as already found using, *e.g.*, RDT [31]. The run with pure stratification shows no energy growth even after being continued for 130 turnover times. On the other hand, for various values of N/f, including in the purely rotating case, a growth is obtained after an initial adjustment phase, and at different rates, as already found in [22,27,30] for $N/f \geqslant 1$. Note that runs with $N/f = 1/2$ and 2 grow with similar rates (highlighted by the shaded region in the plot), while the run with pure rotation grows at a slower pace. Similar results are obtained when studying the evolution of the integral scale as a function of time.

The overall data set is best represented by examining scatter plots. In fig. 2 (bottom) we also show the mean value of $\sigma = \mathrm{d}E_V/\mathrm{d}t$ averaged for $10 \leqslant t/\tau_{\mathrm{NL}} \leqslant 30$. The runs with $1/2 \leqslant N/f \leqslant 2$ show the fastest growth; σ decays monotonically for $N/f > 2$ and is close to zero or becomes negative in the runs with $f = 0$.

To understand the reason for these differences, we consider the flux of kinetic energy from 3D modes to 2D modes,

$$\Pi_{3\mathrm{D}\to 2\mathrm{D}} = \iint \left[\hat{\mathbf{u}}_{\mathbf{k}}^* \cdot \widehat{(\mathbf{u}\cdot\nabla\mathbf{u})}_{\mathbf{k}}\right]_{k_\parallel = 0} \mathrm{d}k_x \mathrm{d}k_y + \mathrm{c.c.}, \quad (5)$$

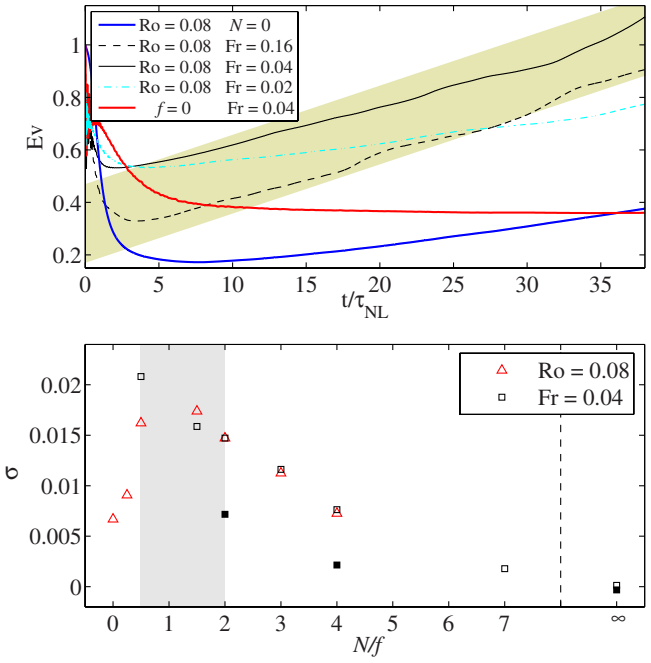

Fig. 2: (Colour on-line) Top: kinetic energy as a function of time for runs with $N/f = 0$, $1/2$, 2, and 4 (all with the same Ro), and for a purely stratified run ($f = 0$). Note the growth of energy after $t/\tau_{\rm NL} \approx 5$ in all runs except in the latter. In several runs with stratification the energy grows faster than in the purely rotating case ($N = 0$). The gray band indicates an average slope observed in the runs with $1/2 \leqslant N/f \leqslant 2$, and highlights runs in which the energy grows faster. Bottom: growth rate σ of $E_V(t)$ as a function of N/f for all runs. Empty symbols correspond to 512^3 runs, and filled symbols to 1024^3 runs. Triangles (red) have constant Ro, while squares (black) have constant Fr. The gray band indicates the range $1/2 \leqslant N/f \leqslant 2$, where the energy grows faster. The dashed vertical line indicates a cut in the data, since there are no data points for $N/f > 7$, except for the point with $f = 0$ (no rotation).

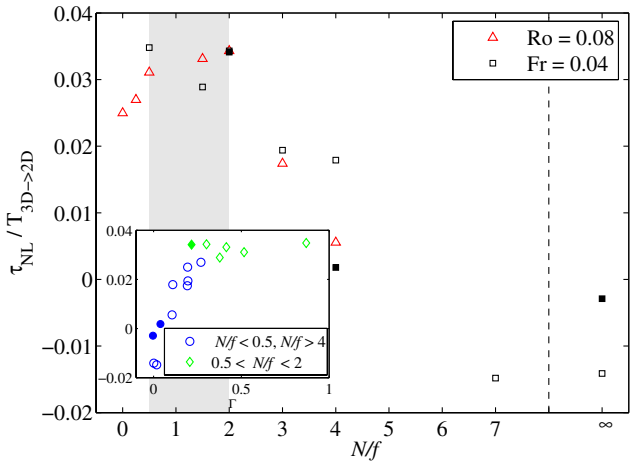

Fig. 3: (Colour on-line) Normalized flux of kinetic energy from 3D modes to 2D modes, as a function of N/f for all the runs. When normalized, the flux corresponds to a dimensionless inverse transfer time from the 3D to the 2D modes. Empty symbols correspond to 512^3 runs, and filled symbols to 1024^3 runs. Runs with $1/2 \leqslant N/f \leqslant 2$ (shaded region) have maximum transfer of energy towards the 2D modes (larger than the run with pure rotation, corresponding to $N/f = 0$), while runs with $N/f \geqslant 7$ have negative transfer (*i.e.*, energy goes towards the 3D modes). The inset shows the same inverse transfer time as a function of the efficiency of the inverse cascade Γ (see text for definition) in all the runs. Runs in the $1/2 \leqslant N/f \leqslant 2$ range are indicated by diamonds, and have the largest efficiencies.

where the hat denotes Fourier transform, the brackets indicate the integrand is evaluated at $k_\parallel = 0$, and the complex conjugate (c.c.) of this integral is added to get a real quantity. When positive, $\Pi_{3D\to2D}$ gives the amount of energy transferred from 3D modes to 2D modes per unit of time, and the direction of the transfer is reversed when $\Pi_{3D\to2D}$ is negative. As the flux has units of energy per unit of time, we can build an inverse transfer time as

$$\frac{1}{T_{3D\to2D}} = \frac{\Pi_{3D\to2D}}{U_F^2}, \qquad (6)$$

and a dimensionless transfer time as $\tau_{\rm NL}/T_{3D\to2D}$. The quantity in eq. (6) is signed, with the sign indicating the direction of the transfer, and when larger it indicates the transfer is faster (*i.e.*, the transfer time is shorter). The dimensionless transfer time for all the runs is plotted as a function of N/f in fig. 3 after averaging over 20 turnover times (for all the runs, $\tau_{\rm NL}/T_{3D\to2D}$ remains approximately constant in time).

Runs with $1/2 \leqslant N/f \leqslant 2$ show the fastest transfer of energy to 2D modes (larger than in the run with pure rotation). For $N/f > 2$, $\tau_{\rm NL}/T_{3D\to2D}$ decreases, and becomes negative (*i.e.*, energy goes from 2D modes to 3D modes) in the purely stratified case. This indicates that the inverse cascade in rotating and stratified flows is associated with a build-up of energy in 2D modes, and that rotation plays an important role in this transfer.

This conclusion is confirmed by the correlation in the growth behavior between kinetic energy (see σ as a function of N/f in fig. 2) and $\tau_{\rm NL}/T_{3D\to2D}$. The inset in fig. 3 shows $\tau_{\rm NL}/T_{3D\to2D}$ as a function of $\Gamma = \sigma/\epsilon$; Γ is a rescaled kinetic-energy growth which we call "efficiency" for short; it is based on σ normalized by the total amount of energy injected in the system, ϵ. The most efficient inverse cascade is for $N/f = 1/2$ (with $\Gamma \approx 0.86$). Indeed, although rotation is necessary to get $\tau_{\rm NL}/T_{3D\to2D} > 0$, moderate stratification helps the inverse cascade (the purely rotating run, with $N/f = 0$, has $\Gamma \approx 0.19$).

The faster growth of large-scale structures in the runs with $1/2 \leqslant N/f \leqslant 2$ (and the associated faster transfer of energy towards 2D modes) is likely due to the fact that, in the presence of stratification, the flow is less anisotropic, with $k_\perp$ and $k_\parallel$ both being populated by the linear (and non-linear) interactions. Note that the range $1/2 \leqslant N/f \leqslant 2$ also corresponds to the range of parameters in rotating and stratified flows for which triadic wave resonances are non-existent [27]. For the case $N/f = 1$,

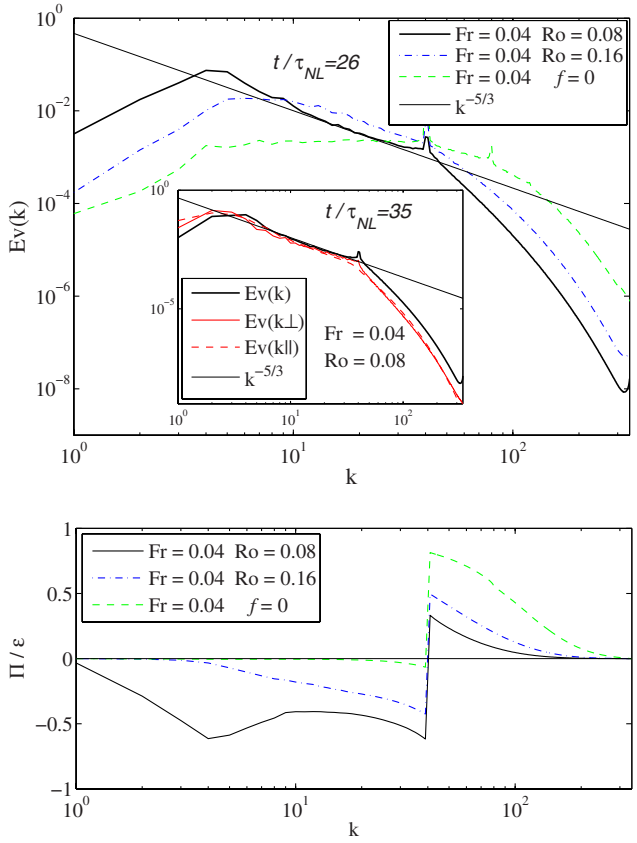

Fig. 4: (Colour on-line) Isotropic kinetic-energy spectra (top) and normalized total energy fluxes (bottom) for three runs on grids of 1024^3 points, with $\mathrm{Re} \approx 10^3$, and Fr and Ro as indicated by the labels. A $-5/3$ slope is given as a reference. The run with pure stratification has a flat spectrum for $k < k_F$. In the inset are the kinetic-energy spectra: isotropic as a function of k, parallel as a function of $k_\parallel$, and perpendicular as a function of $k_\perp$) at a later time in the run with $N/f = 2$. Note the range of wave numbers with negative flux for $k < k_F$ for some of the runs, and that the run with pure stratification has flux close to zero in the same range.

this can be easily verified as the dispersion relation of inertial-gravity waves in (4) reduces to $\omega_{\mathbf{k}} = \pm N$; then, the resonant condition $\omega_{\mathbf{k}} + \omega_{\mathbf{p}} + \omega_{\mathbf{q}} = 0$ can never be fulfilled. The generalization of this argument to the range $1/2 \leqslant N/f \leqslant 2$ is straightforward and can be found in [27]. The absence of resonant interactions in this range may also help coupling 2D and 3D modes (which, for the purely rotating case, may be only weakly coupled or uncoupled, see [34]), and can explain the enhanced transfer from 3D to 2D modes observed in fig. 3. In that range, where resonances are non-existent, only non-linear interactions between eddies can operate, and they efficiently produce an inverse cascade, unimpeded by waves.

Finally, in fig. 4, we show the isotropic kinetic-energy spectra as well as the total energy flux at $t/\tau_{\mathrm{NL}} = 26$ in several runs with 1024^3 grid points, $k_F \approx 40$, and $N/f = 2$, 4, and ∞ (no rotation). We also show a detail of the isotropic, perpendicular, and parallel kinetic-energy spectra for the run with $N/f = 2$ in the inset. The run with $N/f = 2$ has larger scales (evidenced by the peak of the energy spectrum at a smaller k), and in the case with pure stratification the spectrum at large scales has flattened out, a feature already observed by several authors and attributed to the layering of the flow [20], as also observed in the visualization (see fig. 1). Such a flat spectrum has been obtained for purely stratified flows using, as a model for the layered structure, a superposition of delta functions in the vertical [20].

In the two runs with rotation, the inverse cascade is present and it follows a clear $-5/3$ law, as would be the case for a two-dimensional fluid [6]. However, it cannot be discarded that this slope may be dependent on the properties of the forcing, as for the purely rotating case it has been observed that the energy scaling in the inverse-cascade range depends, *e.g.*, on the anisotropy of the forcing [9] (note that in the present study we use isotropic forcing). At late time, in the runs with moderate N/f, there is a clear equipartition between the $k_\perp$ and $k_\parallel$ dependencies, with all spectra displaying a $\sim k^{-5/3}$ scaling.

The spectra at small scale ($k > k_F$) are steep, but insufficient resolution precludes us from making any assessment as to what is the scaling law at these wave numbers. We simply note that in the purely stratified case, there is more energy at small scale than when rotation is present: at a fixed energy input rate, if a measurable amount of energy goes to large scales, less can be transferred to small scales.

The fluxes confirm what is observed in the energy spectra. Again, the lack of adequate scale separation (*i.e.*, the separation between k_F and $k_{\max} = n_p/3$) at small scale leads to positive by not quite constant energy fluxes. However, there is a measurable transfer to small scales (represented by the positive flux), the lesser the stronger the rotation. At large scales ($k < k_F$), the energy flux is negative and tending toward being constant, specially in the run with $N/f = 2$. This range with negative flux is shorter in the run with $N/f = 4$ (and smaller in amplitude), while the purely stratified flow has only a very short range of wave numbers with almost negligible negative flux. As is apparent from the results shown above, this small flux is not enough to give any measurable growth in the overall scale of structures or in kinetic energy. Similar results are obtained for the spectra and fluxes in all the runs with grids of 512^3 points and $k_F \approx 22$.

Conclusion. – We have shown, using 512^3 and 1024^3 simulations of the incompressible Boussinesq equations, that the inverse energy cascade in rotating and stably stratified turbulence is non-monotonic in N/f, and that the combination of rotation with weak stratification (for $1/2 \leqslant N/f \leqslant 2$) results in a faster growth of large scales than in purely rotating flows. This results from an enhanced coupling between 3D and 2D modes (associated with a suppression of resonant interactions), which allows for faster transfer of energy towards 2D motions.

It is interesting that the range identified as with faster growth is compatible with quasi-geostrophic behavior at finite but small Fr [27]. The observed spectrum $\sim k^{-5/3}$ at large scale can thus be interpreted in the light of Charney's theory [24], and the steeper spectrum at small scales is also compatible with such behavior. For future studies, the effect of anisotropic forcing on the cascade is of particular interest as it can have implications for atmospheric and oceanic flows; so is the creation of helicity in such flows [35]. In a different context, that of beta-plane turbulence, it has been shown that the inverse-cascade phenomenon can be arrested at a certain wave number by dispersive waves [36], and an interplay between non-linearities and dispersive waves could explain the behavior observed here for $N/f \gg 1$. Finally, the effect of considering larger buoyancy Reynolds number $\mathcal{R}_B$ in the inverse cascade can be of interest, although more computing power would be required to resolve the inverse-cascade range together with a direct cascade at large $\mathcal{R}_B$.

* * *

This work is supported by NSF/CMG 1025183 and an NSF cooperative agreement through the University Corporation for Atmospheric Research on behalf of NCAR. Computer time was provided by NSF/XSEDE TG-PHY100029 and NCAR/ASD. PDM acknowledges support from PICT Grants Nos. 2011-1529 and 2011-1626.

REFERENCES

[1] Cambon C., *Eur. J. Mech. B*, **20** (2001) 489.
[2] Polzin K. and Lvov Y., *Rev. Geophys.*, **49** (2011) RG4003.
[3] Ivey G. *et al.*, *Annu. Rev. Fluid Mech.*, **40** (2008) 169.
[4] Fox-Kemper B. *et al.*, *Ocean Model.*, **39** (2011) 61.
[5] Cavaleri L. *et al.*, *Bull. Am. Met. Soc.*, **93** (2012) 1651.
[6] Kraichnan R. H. and Montgomery D., *Rep. Prog. Phys.*, **43** (1980) 547.
[7] Tabeling P., *Phys. Rep.*, **362** (2002) 1.
[8] Boffetta G. and Ecke R., *Annu. Rev. Fluid Mech.*, **44** (2012) 427.
[9] Sen A. *et al.*, *Phys. Rev. E*, **86** (2012) 036319.
[10] Celani A. *et al.*, *Phys. Rev. Lett.*, **104** (2010) 184506.
[11] Sorriso-Valvo L. *et al.*, *Phys. Rev. Lett.*, **99** (2007) 115001.
[12] Marino R. *et al.*, *Planet. Space Sci.*, **59** (2011) 592.
[13] Marino R. *et al.*, *Astrophys. J.*, **750** (2012) 41.
[14] Smith L. *et al.*, *Phys. Rev. Lett.*, **77** (1996) 2467.
[15] Lindborg E., *Geophys. Res. Lett.*, **32** (2005) L01809.
[16] Lindborg E. and Brethouwer G., *J. Fluid Mech.*, **586** (2007) 83.
[17] Brethouwer G. *et al.*, *J. Fluid Mech.*, **585** (2007) 343.
[18] Aluie H. and Kurien S., *EPL.*, **96** (2011) 44006.
[19] Waite M., *Phys. Fluids*, **23** (2011) 066602.
[20] Kimura Y. and Herring J. R., *J. Fluid Mech.*, **698** (2012) 19.
[21] Almalkie S. and de Bruyn Kops S. M., *J. Turbul.*, **13** (2012) N29.
[22] Métais O. *et al.*, *Dyn. Atmos. Oceans*, **23** (1996) 193.
[23] Kurien S. *et al.*, *EPL.*, **84** (2008) 24003.
[24] Charney J. G., *J. Atmos. Sci.*, **28** (1971) 1087.
[25] Vallgren A. and Lindborg E., *J. Fluid Mech.*, **656** (2010) 448.
[26] Mininni P. D. and Pouquet A., *Phys. Fluids*, **22** (2010) 035105.
[27] Smith L. and Waleffe F., *J. Fluid Mech.*, **451** (2002) 145.
[28] Laval J.-P. *et al.*, *Phys. Rev. E*, **68** (2003) 036308.
[29] Waite M. and Bartello P., *J. Fluid Mech.*, **517** (2004) 281.
[30] Waite M. and Bartello P., *J. Fluid Mech.*, **568** (2006) 89.
[31] Hanazaki H., *J. Fluid Mech.*, **465** (2002) 157.
[32] Bartello P., *J. Atmos. Sci.*, **52** (1995) 4410.
[33] Mininni P. D. *et al.*, *Parallel Comput.*, **37** (2011) 316.
[34] Cambon C. *et al.*, *New. J. Phys.*, **6** (2004) 73.
[35] Marino R. *et al.*, *Phys. Rev. E*, **87** (2013) 033016.
[36] Legras B. *et al.*, *Phys. Rev. Lett.*, **82** (1999) 4440.